Dynamics of Variable Dusk-Dawn Flow Associated with Magnetotail Current Sheet Flapping

James H. Lane[1], Adrian Grocott[1], Nathan A. Case[1], Maria-Theresia Walach[1]

[1] Department of Physics, Lancaster University, Lancaster, UK

Correspondence to: James Lane (j.lane@lancaster.ac.uk)

Abstract

Previous observations have provided a clear indication that the dusk-dawn ($v_{\perp y}$) sense of both slow (< 200 km s^{-1}) and fast (> 200 km s^{-1}) convective magnetotail flows is strongly governed by the Interplanetary Magnetic Field (IMF) B_y conditions. The related 'untwisting hypothesis' of magnetotail dynamics is commonly invoked to explain this dependence, in terms of a large-scale magnetospheric asymmetry. In the current study, we present Cluster spacecraft observations from 12 October 2006 of earthward convective magnetotail plasma flows whose dusk-dawn sense disagrees with the untwisting hypothesis of IMF B_y control of the magnetotail flows. During this interval, observations of the upstream solar wind conditions from OMNI, and ionospheric convection data using SuperDARN, indicate a large-scale magnetospheric morphology consistent with positive IMF B_y penetration into the magnetotail. Inspection of the in-situ Cluster magnetic field data reveals a flapping of the magnetotail current sheet; a phenomenon known to influence dusk-dawn flow. Results from the curlometer analysis technique suggest that the dusk-dawn sense of the $\boldsymbol{J} \times \boldsymbol{B}$ force was consistent with localised kinks in the magnetic field and the flapping associated with the transient perturbations to the dusk-dawn flow observed by the Cluster 1 spacecraft. We suggest that the IMF B_y penetration at the location of Cluster was unable to override the variable dusk-dawn flow associated with the flapping. We conclude that invocation of the untwisting hypothesis may be inappropriate when interpreting intervals of dynamic magnetotail behaviour such as during current sheet flapping, particularly at locations where magnetotail flaring becomes dominant.

Deleted: Results from the curlometer analysis technique suggest that the dusk-dawn flow perturbations may have been driven by the $\boldsymbol{J} \times \boldsymbol{B}$ force associated with a dawnward-propagating flapping of the magnetotail current sheet, locally overriding the expected IMF B_y control of the flows.

Deleted: , particularly at location where magnetotail flaring becomes dominant.

1. Introduction

Deleted: ¶
¶

Convective magnetotail plasma flows at Earth, driven by the closing of magnetic flux via reconnection as part of the Dungey Cycle (Dungey, 1961) have been studied extensively for many years (e.g. Angelopoulos et al. 1992, 1994; Sergeev et al., 1996; Petrukovich et al., 2001; Cao et al., 2006; McPherron et al., 2011; Frühauff & Glassmeier, 2016). Arguably, the most well studied of these is the Bursty Bulk Flow (BBF). Angelopoulos et al. (1994) defined BBFs as being channels of earthward plasma flow continually above 100 km s^{-1}, exceeding 400 km s^{-1} at one point across some interval, usually across a timescale of a few minutes. The flows are said to be the main transporter of mass, energy and flux in the magnetotail (e.g. Angelopoulos et al., 1994; Nakamura et al., 2002; Grocott et al., 2004a; Kiehas et al., 2018). Although their earthward nature is the key defining characteristic of BBFs, they will invariably exhibit a dusk-dawn component in their bulk flow as well (e.g. Angelopoulos et al., 1994; Petrukovich et al., 2001; Grocott et al., 2004b). Understanding the drivers of dusk-dawn asymmetries in magnetospheric dynamics is an important element of geospace research (e.g. Haaland et al., 2017).

Magnetotail flows are generally expected to be symmetric about midnight, at least in the absence of any asymmetry (e.g. Kissinger et al., 2012). A key factor that has been observed to influence the dusk-dawn direction of the magnetotail flow, however, is the B_y component of the Interplanetary Magnetic Field (IMF). It is well established that when the IMF reconnects with the dayside terrestrial magnetic field, a non-zero IMF B_y component leads to asymmetric loading of open flux into the polar cap (e.g. Khurana et al., 1996; Tenfjord et al., 2015; Grocott et al., 2017; Ohma et al., 2019). This results in a twisting of the magnetotail whereby the closed field lines are rotated about the midnight meridian, and a B_y component is superimposed onto the tail field as a consequence of IMF B_y penetration (Cowley, 1981; Petrukovich, 2011; Tenfjord et al., 2015). Subsequently, following nightside reconnection, the tail will untwist (Grocott et al., 2004c), with the excitation of multiple convective flow bursts, each with an earthward and dusk-dawn component, in the tail and nightside ionosphere (Grocott et al., 2007). In order to be consistent with the tail 'untwisting hypothesis', any convective flows associated with an individual tail field line

should share the same dusk-dawn direction (e.g. see Figure 3 of Grocott et al., 2005). The role of IMF B_y in the untwisting hypothesis has been examined previously in a number of studies (e.g. Grocott et al, 2007; Pitkänen et al., 2013, 2015, 2017). These studies revealed that under prolonged positive IMF B_y conditions, the earthward flows are expected to exhibit a dawnward component in the northern hemisphere ($B_x > 0$) and a duskward component in the southern hemisphere ($B_x < 0$), with the opposite correlation for negative IMF B_y conditions. This is especially true close to midnight, where the penetration of IMF B_y is particularly noticeable. Further away from midnight, however, effects such as magnetotail flaring (Fairfield, 1979) are expected to product a dominant B_y component, which may suppress IMF B_y-effects on the dusk-dawn asymmetry, resulting in the symmetric earthward convection of field lines (e.g. see Fig. 2 of Pitkänen et al., 2019). Nevertheless, IMF B_y has been shown to govern the dusk-dawn nature of these flows both during periods of steadier, slower convection (Pitkänen et al., 2019), as well as during more transient, dynamic BBF-like intervals (Grocott et al., 2007) at up to 7 R_E towards the dusk-dawn flanks (Pitkänen et al., 2013). In the present study, we present Cluster observations of dawnward and duskward directed flows that do not match this expected dependence on IMF B_y, implying that the untwisting hypothesis is insufficient in this case. In particular, we highlight the problematic nature of the observation of dawnward flow, in relation to the pre-midnight location of Cluster. We instead suggest that the flows are being driven by local perturbations due to dynamic behaviour of the tail that are associated with flapping of the current sheet.

The current sheet, or 'neutral' sheet, lies in the equatorial plane at the center of the tail plasma sheet and separates the earthward ($B_x > 0$) and tailward ($B_x < 0$) directed field (Ness, 1965). The current sheet is a highly dynamic region of the Earth's magnetotail which can undergo various types of net motion, such as tilting due to lobe magnetic pressures (Cowley et al., 1981; Tenfjord et al., 2017) as well as flapping. Flapping of the current sheet can generally be described as a sinusoidal-like variation in B_x of up to tens of nanoTesla, where an observing spacecraft often measures repeated changes in the sign of B_x (e.g. Runov et al., 2009), indicative of crossings of the current sheet, with characteristic times ranging from a few seconds to (more commonly) several minutes (e.g. Runov et al., 2009; Wu et al., 2016; Wei et al., 2019). Drivers of current sheet flapping have been widely investigated, with possible causes ranging from external solar wind/IMF changes (Runov et al., 2009),

Formatted: Font: Italic

Formatted: Font: Italic, Subscript

Deleted: ; Pitkänen et al., 2013

Deleted:

Deleted: I

Deleted: , we

induction of hemispheric plasma asymmetries (Malova et al., 2007; Wei et al., 2015), fast earthward flow (Nakamura et al., 2009) as well as periodical, unsteady magnetotail reconnection (Wei et al., 2019). Studies such as Volwerk et al. (2008) and Kubyshkina et al. (2014) have illustrated that flapping of the current sheet can be associated with variable dusk-dawn flow, potentially overriding, or preventing any IMF B_y control of the flow.

In this paper we present Cluster spacecraft observations of an interval of dynamic magnetotail behaviour on 12 October 2006. Throughout this interval, Cluster 1 observed oscillations in the magnetic field B_x component, which we attribute to current sheet flapping, concurrent with a series of convective fast flows with significant and variable dusk-dawn components. The B_y component of the concurrent upstream IMF had been largely positive for several hours prior to the flapping. Consequently, the interval discussed here provides an opportunity to investigate the possible competition of two distinct mechanisms for control of the dusk-dawn flow: 1) IMF B_y and 2) localized dynamics related to the flapping of the current sheet. In contrast to studies which have come before such as those presented by Grocott et al. (2007) and Pitkänen et al. (2015), the observed dusk-dawn direction of transient flow enhancements in this case disagrees with that which might be expected from the prevailing IMF B_y conditions, despite clear evidence for global penetration of positive IMF B_y. We therefore suggest that IMF B_y penetration at the location of Cluster was unable to overcome the variable dusk-dawn flow associated with the flapping.

Deleted: We therefore suggest that flapping of the current sheet had locally overridden the IMF B_y control of the dusk-dawn flow observed by Cluster 1.

2. Instrumentation and Data Sets

2.1. Spacecraft Data

The magnetospheric observations presented in this case study were made by the Cluster multi-spacecraft (C1-C4) constellation (Escoubet et al., 2001). We make use of the fluxgate magnetometer (FGM) onboard the Cluster spacecraft to obtain magnetic field measurements (Balogh et al., 2001), and obtain our bulk ion velocity data from the Hot Ion Analyser (HIA) on C1 and C3 calculated as on-board moments (Rème et al., 1997). The magnetic field data presented are 5 vectors-per-second (0.2s res) which have been 1s median-averaged, with the velocity data presented having spin resolution of just over 4s. Where these datasets have been combined to produce parameters such as the plasma beta

and field-perpendicular velocities, we have resampled both the magnetic field and plasma data to 5s resolution. All data are presented in geocentric solar magnetospheric (GSM) coordinates unless stated otherwise.

The interval of study in this paper occurred between 00:00 – 00:55 UT on 12 October 2006. At 00:00 UT the Cluster spacecraft were located in the near-Earth magnetotail plasma sheet, in the pre-midnight sector. C1 was located at (X = −14.7, Y = 6.0, Z = −1.2) R_E, C2 at (X = −14.2, Y = 7.5, Z = −0.7) R_E, C3 at (X = −13.9, Y = 7.0, Z = −2.1) R_E, and C4 at (X = −13.2, Y = 6.2, Z = −0.8) R_E. This is depicted in Fig. 1a by the colored triangles, along with the respective spacecraft trajectories, from 00:00 – 00:55 UT, by the solid lines. Fig. 1b shows a zoomed-out version of Fig. 1a, which illustrates the location of the spacecraft with respect to the Earth. Fig. 1b also shows a traced modelled magnetic field line, achieved using the semi-empirical TA15 model of the magnetosphere (Tsyganenko & Andreeva, 2015), which passes through the location of C1 and connects to both the northern and southern hemispheres of the Earth. We parameterised the TA15 model using mean-averaged solar wind dynamic pressure (P_{dyn}), IMF B_y and IMF B_z data from the 1-hour interval prior to 00:28 UT (the start of our specific interval of interest). These values were P_{dyn} = 1.56 nPa, IMF B_y = +1.56 nT and IMF B_z = -2.17 nT. There was also a tailward dipole tilt of ≈-12°. The model was also parameterised with a solar wind coupling function index known as the 'N index', after Newell et al. (2007). The N index varies between 0 (quiet) and 2 (very active), and in this instance was ~0.4.

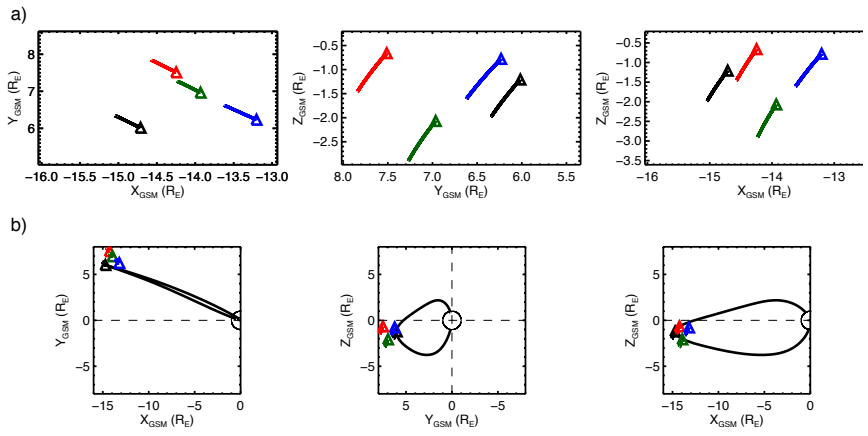

Deleted: ure

Deleted: ure

Deleted: ure

Deleted: ure

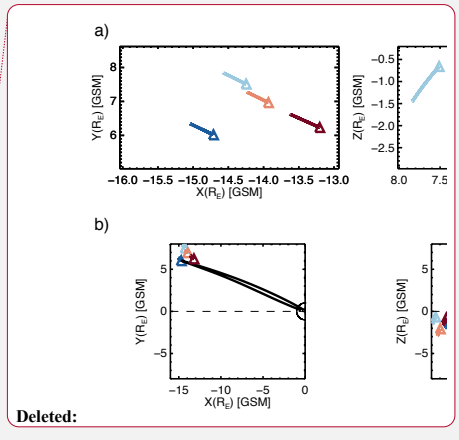

Deleted:

Figure 1: a) The locations of the Cluster spacecraft in the X-Y, Y-Z, and X-Z GSM planes, from left to right, respectively, at 00:00 UT on 12 October 2006, marked by the triangles. The trajectories from 00:00 UT to 00:55 UT are marked by the solid lines. The spacecraft are color-coded according to the key on the right. b) As in a), with a zoomed-out view. The Earth is shown by the solid circle. A TA15 model magnetic field line passing through the location of C1 is shown as the solid black line.

The IMF measurements used in this study were provided by the OMNIweb database at 1-minute resolution, having been first propagated from L1 to the bow shock nose (King & Papitashvili, 2005).

2.2. SuperDARN Data

The ionospheric observations presented in section 3.3 were provided by the Super Dual Auroral Radar Network (SuperDARN), an international collaboration of 36 ground-based radars (Nishitani et al., 2019) that make line-of-sight Doppler measurements of the horizontal motion of the ionospheric plasma every few seconds (e.g. Chisham et al., 2007). Here, we use 2-min ionospheric convection maps created by fitting the line-of-sight **E** x **B** velocity data to an eighth order expansion of the ionospheric electric potential in spherical harmonics using the technique of Ruohoniemi & Baker (1998), implemented in the Radar Software Toolkit (RST version 4.2, 2018). To accommodate intervals with limited data availability, the data are supplemented with values derived from a statistical model parameterized by IMF conditions. This is a well-established technique that has been thoroughly discussed by, e.g., Chisham et al. (2007). The convection maps we present employ the commonly used model of Ruohoniemi & Greenwald (1996). As a check on the sensitivity of the maps to the choice of model input, we also tested the fitting using the alternative model of Thomas and Shepherd (2018) and found that this has little impact on the maps and no impact on our conclusions.

As a further measure to ensure that the choice of model is not critical to our results, we chose not to use the concurrent IMF vector to parameterise the background model. In this case, because we are using the SuperDARN data to provide evidence in support of the expected large-scale influence of IMF B_y, we deemed it inappropriate to include model data

already parametrised by IMF B_y. We instead specify a nominal southward IMF with zero B_y component in our analysis, to ensure that a background model with no pre-existing IMF B_y influence is used. Although this might result in the patterns we show being less accurate overall, especially in regions of poor data coverage, it will ensure that any B_y-associated asymmetry in the maps is driven by the radar data from our interval of study, and not the background model. This is discussed further in section 4.1, below.

3 Observations

In this section we present observations of the IMF, magnetotail magnetic field and plasma flow, and ionospheric convection from an interval on 12 October 2006.

3.1 IMF Observations

Figure 2 presents an overview of the spacecraft data from an extended interval around our period of specific interest for broader context. In Figure 2a, we show a time-series of the IMF B_y and IMF B_z data from 20:00 UT on 11 October to 01:00 UT on 12 October 2006. These data reveal that IMF B_y was generally positive for several hours prior to the fast flow interval, with IMF B_z predominantly negative. There were three small intervals of negative IMF B_y at ~ 21:35 UT, 23:00 UT and 23:40 UT and we discuss the possible ramifications of these, and our treatment of them, in section 4.1.

3.2 Cluster Spacecraft Observations

In Figure 2b, we present the in-situ magnetic field and plasma measurements from the Cluster spacecraft across the interval 00:00 – 00:55 UT.

Deleted: ¶
¶
¶
¶

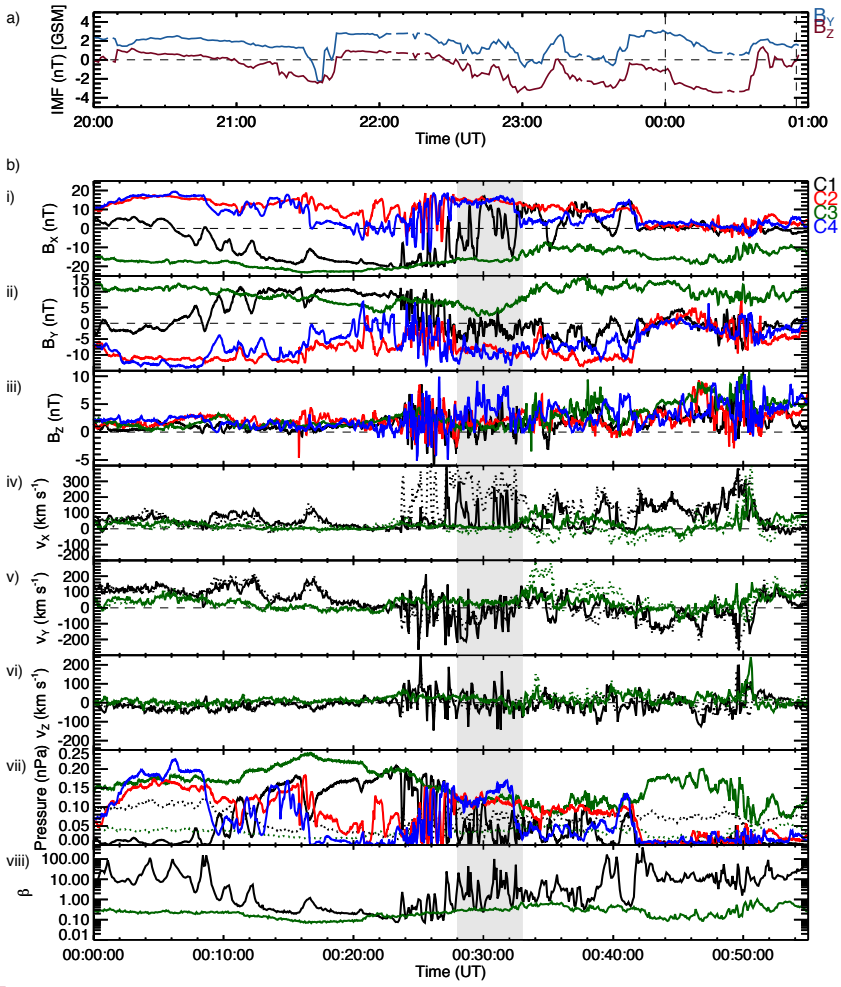

Deleted:

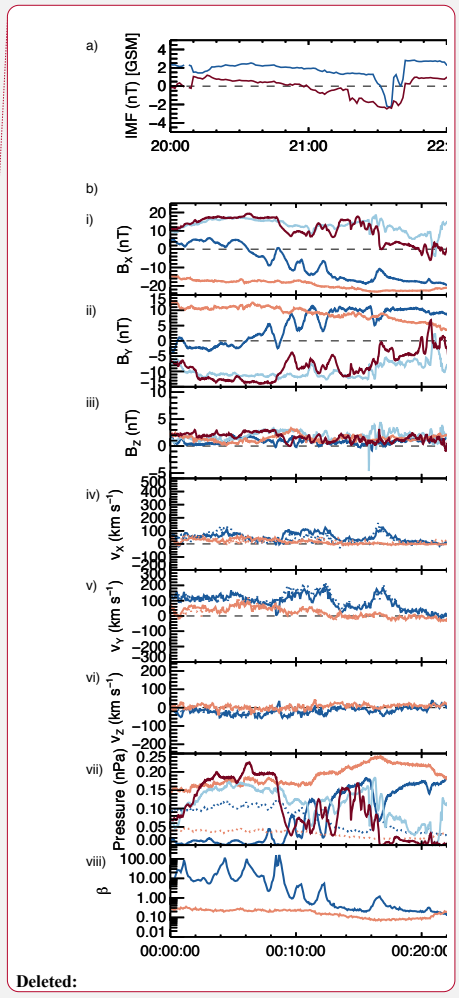

Figure 2: a) A plot of the IMF time series data for the IMF B_y (blue) and IMF B_z (red) components, from 20:00 UT on 11 October 2006 to 01:00 UT on 12 October 2006. The vertical dashed lines indicate the start (00:00 UT) and end (00:55 UT) of the interval of Cluster data (below). b) The in-situ Cluster spacecraft measurements. Shown first is the local magnetic field data, i) B_x, ii) B_y and iii) B_z, followed by the bulk ion velocity data, iv) v_x, v) v_y, and vi) v_z (dotted lines). The field-perpendicular component of the ion flow (indicative of the **E x B** convection) is shown in panels iv) to vi) by the solid lines. In panel vii) the magnetic

$\left(\frac{B^2}{2\mu_0}\right)$ and thermal ion (nkT) pressures are shown by the solid and dotted lines respectively, and in panel viii) the ion plasma beta from C1 and C3 is shown. All data are labelled according to the color-coded key on the right-hand side. The time-interval between the gray shaded region marks our specific interval of interest (discussed in text).

At ~00:06 UT, C1 crossed from the northern hemisphere into the southern hemisphere, illustrated by the sign change in B_x from positive to negative shown in Fig. 2b i). Coincident with this, the observed B_y, shown in Fig. 2b ii) turned from negative to positive, consistent with the expected B_y due to magnetotail flaring (see section 4.2) at this pre-midnight location (Fairfield, 1979). Fig. 2b iv) reveals that up until ~00:24 UT, the bulk earthward flow (v_x, dotted lines) and field-perpendicular flow ($v_{\perp x}$, solid lines) measured by both C1 and C3 was generally low in magnitude (< 100 km s^{-1}). The dusk-dawn (v_y) component of the flow, shown in Fig. 2b v), remained steadily duskward ($v_y > 0$) at C1 and duskward or close to zero at C3. The north-south (v_z) component of the flow in Fig. 2b vi), measured by C1 and C3 was effectively zero. During this period, the Cluster spacecraft that resided in the northern hemisphere (predominantly C2 and C4), observed $B_y < 0$, and the spacecraft which resided in the southern hemisphere (predominantly C1 and C3) observed $B_y > 0$, again consistent with magnetotail flaring. Occasionally a spacecraft encountered the current sheet ($B_x = 0$) at which point it observed $B_y = 0$. We comment on the significance of these magnetic field observations in section 4.2.

After ~00:24 UT, C1 began to observe a period of enhanced earthward flow (v_x > 300 km s^{-1}) and variable dusk-dawn flow, concurrent with sudden variation in the local B_x component. Similarly, C2 and C4, but not C3, observed large magnitude (> 20 nT) rapid variations in B_x, which appear to have an apparent timescale of around a minute and which we attribute to a flapping of the current sheet. As well as rapid variations in B_x, both the B_y and B_z components of C1, C2 and C4 seemed highly variable. As perhaps to be expected, these variations in the magnetic field were accompanied by significant variations in the magnetic pressure of ~0.15 nPa, as shown by the solid lines in Fig. 2b vii).

Deleted: ure
Deleted: ure
Deleted: ure
Deleted: (v_x
Deleted: gure
Deleted: d ($v_y > 0$) at
Deleted: .
Deleted: ure
Formatted: Font: Not Italic
Formatted: Font: Not Italic
Deleted: .
Deleted: ure

Unlike the other spacecraft, C3 remained in the southern hemisphere throughout the entire interval and did not observe the rapid fluctuations in B_x. Between 00:28 – 00:33 UT (the gray shaded region), C1 began to repeatedly and rapidly cross the current sheet, as previously experienced by C2 and C4, whilst continually observing enhanced earthward flow and variable dusk-dawn convective flow ($v_{\perp y}$). Across the entire interval, the plasma beta, β, indicated in Fig. 2b viii), measured by C3 remained above ~0.1, with C1's measured β ranging from 0.1 to over 100. This is consistent with the fact that C1 was continually crossing the current sheet at the center of the plasma sheet, where β is larger (Baumjohann et al., 1989). It is this interval of current sheet crossing and variable flow observed by C1 that we focus on below and is presented in more detail in Figure 3.

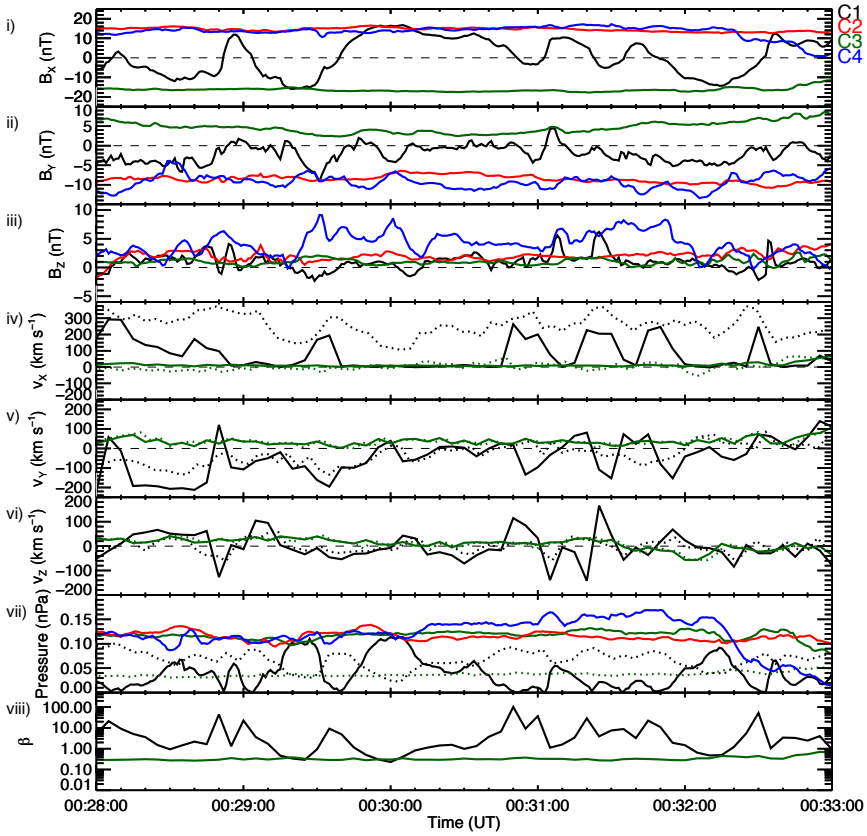

Figure 3: As in Fig. 2b, but for the interval 00:28 – 00:33 UT on 12 October 2006.

Fig. 3 i) conveys the extent of the large-amplitude B_x variations observed by C1 between 00:28 and 00:33 UT. B_x was generally fluctuating between positive and negative values throughout the five-minute interval, with a minimum at ~ −16 nT and maximum at ~17 nT. The magnetic pressure at C1 shown by the solid black line in Fig. 3 vii) is consistent with the idea that C1 was crossing the current sheet, as this generally reached minima at the center of each current sheet crossing ($B_x \approx 0$). The B_y component (Fig. 3ii) measured by C1 generally remained negative and highly variable for the entire interval, with a number of large negative enhancements and a few small positive excursions. It is particularly of note that when C1 was below the neutral sheet, as implied by a negative B_x component, B_y was almost always negative. As we discuss in section 4.2, this is inconsistent with what we would expect based on the location of the spacecraft and also inconsistent with any expectation that a positive IMF B_y should have penetrated into the tail. The B_z component (Fig. 3iii) generally remained positive with some small negative excursions.

Unlike C1, C2-4 measured generally steady B_x throughout this five-minute period. C2 and C4 measured positive B_x, indicating that they were above the neutral sheet, and C3 measured negative B_x, indicating that it was below the neutral sheet. Similarly, B_y was steadily negative for C2 and C4 and steadily positive for C3. Again, we note the inconsistency between the C1 and C3 observations of B_y; when in the southern hemisphere C1 generally observed $B_y < 0$, whereas C3 observed $B_y > 0$. On a few separate occasions C1 did briefly observe $B_y > 0$ (e.g. at 00:31:05 UT) but at these times C1 was located above the neutral sheet ($B_x > 0$), while C2 and C4 observed $B_y < 0$ above the neutral sheet. These variations in B_y imply the observation of a 'kink' in the field at the location of C1, the ramifications of which are discussed further in section 4.2.

At times when B_x observed by C1 was negative, indicating that C1 was below the neutral sheet, C1 generally observed negative (dawnward) $v_{\perp y}$ (Fig. 3v) with a magnitude varying between 100 and 200 km s^{-1}. At times when B_x became positive, indicating that C1 was above the neutral sheet, C1 observed positive (duskward) $v_{\perp y}$ a majority of the time, although this flow barely reached 100 km s^{-1}. The negative enhancements in $v_{\perp y}$ were

Deleted: ure

Deleted: ue

Deleted: ure

Deleted: C1 tended to observe positive (duskward) $v_{\perp y}$,

Deleted: (both positive and negative)

generally accompanied by negative enhancements in B_y. Across the interval, there was a near continual v_x > 200 km s^{-1} flow (black dotted line in Fig. 3iv), peaking at almost 400 km s^{-1}, with concurrent peaks in the convective $v_{\perp x}$ component (solid black line) of at least 200 km s^{-1}. The convective flow measured by C3, however, was generally very weak ($|v_\perp|$ < 50 km s^{-1}) throughout this period (solid green line in Fig 3iv). v_z (Fig. 3vi), as measured by both C1 and C3 remained low in magnitude (< 100 km s^{-1}) for the duration of the interval, with a few $v_{\perp z}$ excursions above 100 km s^{-1} observed by C1. The most significant enhancements in $v_{\perp z}$ seen by C1 appeared to occur in conjunction with the rapid current sheet crossings between 00:30:50 and 00:32:00 UT. We discuss the implications of these observations in the context of the upstream IMF conditions and large-scale magnetospheric morphology in section 4.

3.3 Ionospheric Convection Observations

To provide the large-scale context in which we can interpret the more localized observations from the Cluster spacecraft we show ionospheric convection observations in Figure 4. In Fig. 4a we present a series of four 2-minute integration SuperDARN maps of the northern hemisphere ionospheric convection pattern, beginning at 00:24 UT, and ending at 00:34 UT, which encompasses our specific interval. In all maps, plasma is flowing anti-sunward across the polar cap at high latitudes, also with a strong duskward sense, with the direction of the convection reversing in the pre-midnight sector before returning sunward at lower latitudes.

Deleted: ue

Deleted: ue

Deleted: orange

Deleted: ure

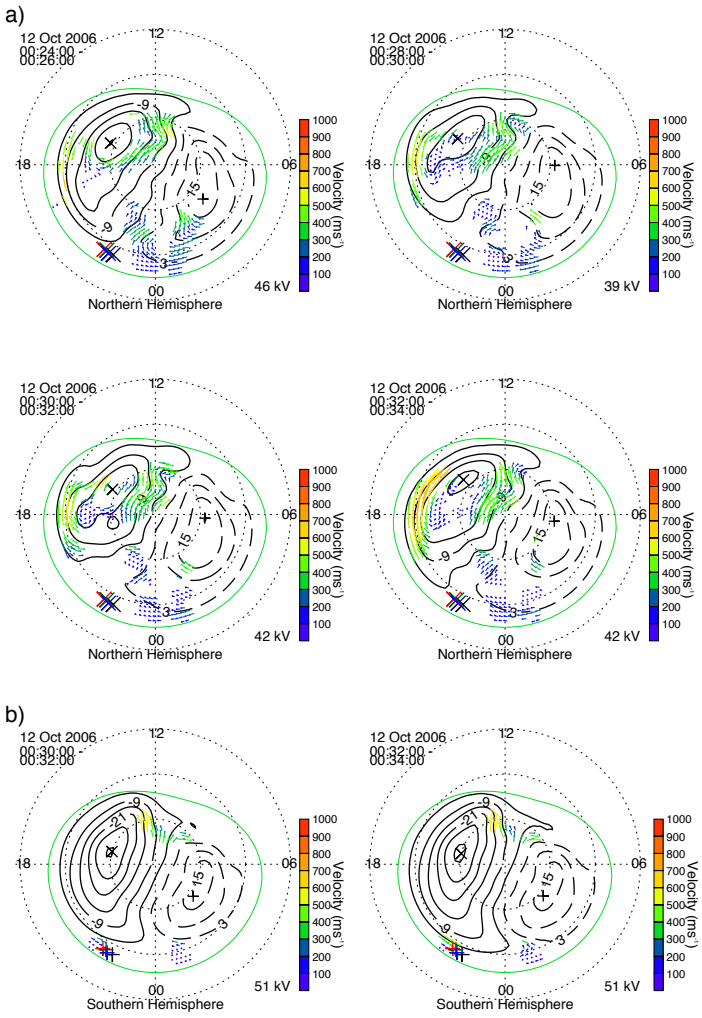

Deleted:

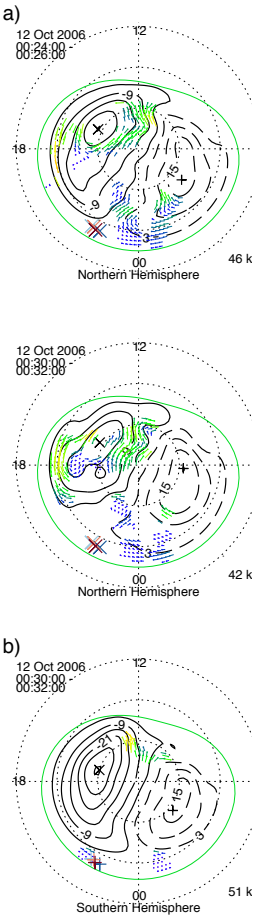

Figure 4: Maps of the ionospheric plasma convection derived from SuperDARN observations. Midnight is to the bottom of each map, noon to the top, dusk to the left and dawn to the right. The dashed black circles are spaced every 10° in magnetic latitude. The thicker solid and dashed black lines represent the plasma streamlines and are the contours of the electrostatic potential. Flow vectors are plotted at the locations of radar observations and these are color-coded based on the magnitude of their velocity. a) Four 2-minute northern hemisphere maps from 00:24 – 00:26, 00:28 – 00:30, 00:30 – 00:32 and 00:32 –

Formatted: Font: +Body (Calibri)

Formatted: Font: +Body (Calibri)

Formatted: Font: +Body (Calibri)

Formatted: Font: +Body (Calibri)

00:34 UT, respectively. b) Two 2-minute southern hemisphere maps from 00:30 – 00:32 and 00:32 – 00:34 UT, respectively. On each northern (southern) hemisphere map, the footpoints of the Cluster spacecraft constellation are shown by the X's (+'s), mapped using the TA15 model.

Owing to the coupled nature of the magnetosphere-ionosphere system, the observed ionospheric convection pattern is indicative of the global-scale magnetospheric convection (Cowley, 1981). In this case, the typical symmetrical twin-cell convection pattern has been rotated clockwise, with the dawn cell extending across into the pre-midnight sector, indicative of convection that has been driven under the influence of a positive IMF B_y component (e.g. Reistad et al., 2016, 2018). On each northern hemisphere map, the footpoints of the Cluster spacecraft constellation are indicated by the crosses (X), mapped using the TA15 model with the same parameterisation described in section 2.

Fig. 4b shows two 2-minute integration SuperDARN maps of the southern hemisphere ionospheric convection pattern, beginning at 00:30 UT, and ending at 00:34 UT. The associated footpoints of the Cluster spacecraft are indicated by the plus signs (+). Although the coverage of radar data is much less than in the northern hemisphere, there are data in the pre- and post-midnight sectors which appears to be influencing the location of the flow reversal region at the nightside end of the dusk cell. Opposite to the northern hemisphere case, it is the dusk cell in the south which is extending towards, or just beyond, the midnight meridian. This is also consistent with a large-scale positive IMF B_y influence, owing to the expected north-south asymmetry of the influence of IMF B_y in the magnetosphere (e.g. Pettigrew et al., 2010). The significance of these observations is further discussed in section 4.1.

Deleted: ure

4. Analysis and Discussion

We have presented observations of a dynamic interval of plasma flows and magnetic field in the Earth's magnetotail. In this section we discuss our rationale for interpreting the flows as

being inconsistent with large-scale magnetotail untwisting and our interpretation of their relationship to current sheet flapping.

4.1 Evidence for an inconsistency with large-scale magnetotail untwisting

During the five-minute interval studied (00:28 – 00:33 UT) C1 measured a continually fluctuating B_x component (Fig. 3i), indicative of multiple crossings of the tail current sheet. C1 was the only spacecraft to measure this signature across the interval (although similar signatures had been observed a few minutes earlier by C2 and C4). C1 also measured a series of earthward convective magnetotail fast flows with varying dusk-dawn components. The data in Fig. 3 i) and Fig. 3 v) illustrate that when B_x was positive (negative), a duskward (dawnward) $v_{\perp y}$ was generally observed. Additionally, the data in Fig. 3 ii) show that C1 tended to observe a negative B_y component. According to the magnetotail untwisting hypothesis (e.g. Pitkänen et al., 2015), these flow and magnetic field observations are consistent with a negative IMF B_y penetration. The IMF data presented in Fig. 2a, on the other hand, revealed that IMF B_y was generally positive for several hours prior to the fast flow interval (00:28 – 00:33 UT). Based on the IMF data alone, therefore, one might expect that a positive IMF B_y will have penetrated into the magnetosphere and thus ought to have determined the "expected" dusk-dawn direction of the flow. In that case, the flows observed here would have a dusk-dawn sense that is not explained by current theoretical models of magnetotail untwisting, meaning they are not IMF B_y-controlled (e.g. Grocott et al., 2007). There are a number of possible explanations for this discrepancy and we address each one in turn.

The first possibility is that our conclusion regarding the expected sense of IMF B_y-control is incorrect. As discussed above, the flows observed by Cluster would be consistent with the magnetotail untwisting hypothesis in the case that we had IMF $B_y < 0$ penetration. We noted in section 3.1 that there were three small negative IMF B_y excursions prior to our Cluster observations interval. Although the propagation of the IMF to the bow shock is accounted for in the OMNI data, there is uncertainty regarding the time it takes for the IMF B_y to 'propagate' into the magnetotail. Uncertainties in IMF B_y propagation times (e.g. Case & Wild, 2012) have previously been cited as an explanation for observing an unexpected asymmetry (e.g. Pitkänen et al., 2013). Studies such as Tenfjord et al. (2015, 2017) and Case

Deleted: ure
Deleted: ure
Deleted: ure
Deleted: ure
Deleted:
Deleted:
Deleted: what is
Deleted: dusk-dawn asymmetry
Formatted: Font: Italic
Formatted: Font: Italic, Subscript

et al. (2018), for example, have suggested a reconfiguration time (to the prevailing IMF B_y conditions) for nightside closed field lines of around 40 minutes. At ~00:28 UT (the beginning of our specific interval of interest), the IMF B_y had been positive for around 50 minutes. Based on the Tenfjord timescale, this would thus imply that our interval was wholly IMF $B_y > 0$ driven. Other studies, on the other hand, such as Browett et al. (2017), have shown that longer timescales of a few hours may be important.

However, for such long timescales to play a role one would expect to have observed a relatively persistent IMF B_y component during that time. The integrated IMF B_y over the hours prior to our interval was certainly convincingly B_y-positive, and it seems highly unlikely that a few minute-long fluctuations into the opposite IMF B_y polarity, 1 or 2 hours prior to the flows we observed, could have a significant influence. We can thus be confident that positive IMF B_y was governing the global magnetospheric dynamics in this case.

Despite this convincing argument that the IMF data alone imply a positive IMF B_y penetration, we performed an additional analysis to further ensure that these negative excursions did not lead to a change in the global nature of the magnetosphere-ionosphere system. We inspected the concurrent northern hemisphere SuperDARN data (presented in Fig. 4a) to provide evidence of the large-scale convection pattern. If the large-scale flow is consistent with a positive IMF B_y component, then the magnetotail flows that we observed must be deviating from this for some reason and cannot be related to IMF B_y-control. The SuperDARN data indeed confirm that the large-scale morphology of the system was consistent with a positive IMF B_y component (e.g. Lockwood 1993; Grocott et al., 2017; Reistad et al., 2018). This can be inferred from the general shape of the convection pattern, whereby across multiple maps (00:24 – 00:34 UT) the pattern was rotated clockwise, with the dawn cell having extended into the pre-midnight sector. That this is the expected convection pattern for an IMF B_y-driven magnetosphere is also supported by the concurrent low level of geomagnetic activity. The auroral AU and AL indices (not shown) confirm that this interval is geomagnetically quiet (AU and |AL| both less than (or of the order of) 10 nT), such that the nightside ionospheric convection asymmetry should be driven by IMF B_y rather than conductivity-driven features such as the Harang reversal which might otherwise

Deleted: ure

Formatted: Font: Italic

Formatted: Font: Italic, Subscript

Deleted: discontinuity

complicate the auroral zone flows (e.g. Grocott et al., 2007; Grocott et al., 2008; Reistad et al., 2018).

The validity of the convection observations is further supported by the coverage of nightside data which were used to constrain the model convection pattern. The data used to create a SuperDARN convection map are supplemented by data from a statistical model (in this case Ruohoniemi & Greenwald, 1996) which is typically parameterised by the instantaneous IMF conditions. In the case that there is a lack of real data coverage, a created SuperDARN map will be strongly influenced by the model data, as opposed to real data, and thus would reflect a prediction of convection based on the IMF conditions. The maps shown in Fig. 4a illustrate that there were dozens of SuperDARN vectors in the midnight sector which were fitted to create the global convection maps. To confirm that these data were sufficient, and that the observed large-scale convection pattern was not being driven by model data, we parameterised the model in our analysis with IMF $B_y = 0$. Despite this, a clear IMF B_y-asymmetry exists, thus demonstrating that the observed large-scale IMF $B_y > 0$ global convection patterns must be data-driven.

A second possible explanation for the discrepancy between the dusk-dawn direction of the local and global-scale convection concerns the certainty with which we can determine the location of the spacecraft with respect to the large-scale convection pattern. The untwisting hypothesis, as considered by e.g. Pitkänen et al. (2013, 2017), relies on the assumption that the convection cell to which the spacecraft is connected should be a factor of only hemisphere and the sense of IMF B_y. In other words, as discussed above, for IMF $B_y > 0$, the hypothesis dictates that C1 ought to be located on the dawn cell when above the neutral sheet and the dusk cell when below, at least in the case that the spacecraft is close to midnight (Grocott et al., 2007). This might be true statistically, but does not account for the dusk-dawn location of the spacecraft, which in this case was $6 \lesssim Y \lesssim 7\ R_E$. If, as a result, the spacecraft was actually located on the dusk cell when above the neutral sheet, and on the dawn cell when below the neutral sheet, then the sense of the observed plasma sheet flows would actually be consistent with the large-scale convection.

Deleted: ure

Moved (insertion) [1]

Deleted: (

Deleted: ,

Deleted: ,

Deleted:)

Moved up [1]: (e.g. Pitkänen et al., 2013, 2017)

Deleted: it is not clear how valid an assumption it might be when trying to interpret observations from a single event in the presence of a highly dynamic neutral sheet. It also fails to

Deleted:

One way to specify which cell the spacecraft is located within is to map its location into the ionosphere. This has been done using TA15 and is shown by the crosses (X) on the northern hemisphere convection maps and by plus signs (+) on the southern hemisphere convection maps, in Fig. 4a and 4b, respectively. Consider first the northern hemisphere map from 00:30 – 00:32 UT in Fig. 4a: the spacecraft appear to map closer to the dawn cell than the dusk cell, such that the predominantly duskward flow that C1 observed in the northern hemisphere plasma sheet would seem to be inconsistent. However, it is worth considering that the pre-midnight location of the spacecraft, the proximity of the mapped footpoints to the dusk cell, and the level of uncertainty generally accepted to be present in field line mapping, may give credence to the possibility that the spacecraft actually mapped to the dusk cell in the northern hemisphere. If this was the case, then the northern hemisphere flows observed by C1 would actually be consistent with the large-scale convection pattern. However, if we consider the southern hemisphere maps in Fig. 4b we can be more certain of which cell the spacecraft map to. Owing to the IMF B_y positive nature of the convection (i.e. the more extended southern hemisphere dusk cell) and the pre-midnight location of the spacecraft, the footpoints are located quite convincingly on the dusk cell. This is despite the dusk-dawn asymmetry being less pronounced than that seen in the northern hemisphere (and the associated poorer coverage of southern hemisphere SuperDARN data). When below the neutral sheet C1 observed dawnward flows, meaning it would have to have been on the southern hemisphere dawn cell to be consistent with the large-scale convection, which is clearly not the case. Indeed, the observed dawnward flow in the southern hemisphere at this location could only be interpreted in terms of the untwisting hypothesis for a situation where we had clear IMF $B_y < 0$ penetration (and associated extended dawn cell), which has already been ruled out. C3, meanwhile, continually observed duskward flow, which appears to be consistent with the larger-scale convection. It seems much more likely, therefore, that C1 observed flow that was associated with localized magnetic field dynamics rather than being a signature of the large-scale convection.

Deleted: ures

Deleted: ure

Deleted: there

Deleted: ure

Deleted:

4.2 Evidence for a local perturbation in the magnetotail

The lack of consistency with the large-scale convection leads us to a third explanation for our observations, which is that there is a local perturbation within the tail that is

552 independent of any large-scale, IMF B_y-controlled asymmetry associated with magnetotail
553 untwisting. This is supported by the observations from the other Cluster spacecraft. The
554 low-level of flow seen by C3 is mostly duskward (Fig. 3v) and therefore consistent with the
555 idea of untwisting under IMF $B_y > 0$, given its southern hemisphere location; although, it
556 should be noted that this observation would also be consistent with the expected duskward
557 flow in a pre-midnight location even in the absence of a large-scale asymmetry (e.g.
558 Kissinger et al., 2012). Further, in Fig. 2b v), up until the rapid B_x variations began at ~00:24
559 UT, fast duskward flow in the southern hemisphere was also seen by C1. The fact that C3
560 continued to then observe steady duskward flow, and no significant B_x change, suggests
561 that the change in the nature of the C1 observations after 00:24 UT must in-fact be due to
562 some localized process that was responsible for driving the dawnward component of the
563 flows which was only observed by C1.
564
565 This idea of a local perturbation is also supported by the variations in the local B_y
566 component. Fig. 3 ii) illustrates the in-situ variations in B_y with time across the interval.
567 Despite there clearly being positive IMF B_y penetration globally (as confirmed by inspection
568 of the OMNI and SuperDARN data), C1, C2 and C4 all recorded mostly negative local B_y
569 values. In the studies of, e.g., Pitkänen et al. (2013, 2017) this observation would have been
570 offered as evidence of a negative of IMF B_y penetration, thus supporting the untwisting
571 hypothesis. However, it is important to note that a negative local B_y component may be
572 wholly consistent with positive IMF B_y. There are, in fact, multiple sources of B_y in the tail,
573 such as magnetotail flaring (Fairfield, 1979), as well as tilt effects and current sheet warping
574 (see e.g. Petrukovich et al., 2005), in addition to a penetration of the IMF B_y. To fully
575 interpret the magnetic field observations, we must therefore consider the possible effects
576 of these phenomena on the presence of B_y in the tail at the specific location of each
577 spacecraft.

Deleted: .

Deleted: ure

Deleted: ure

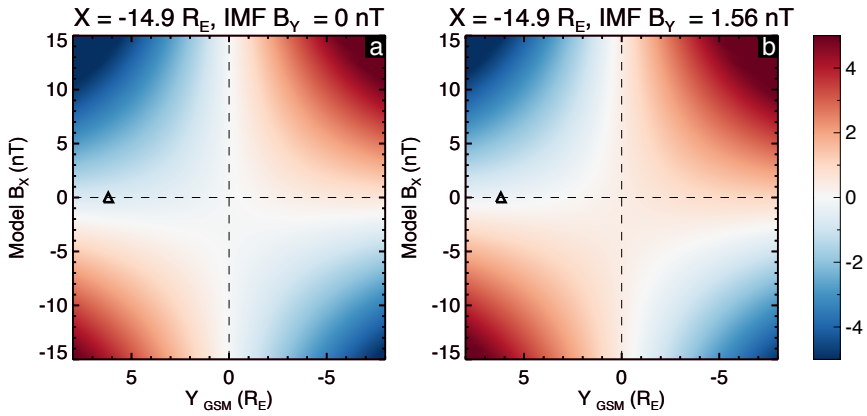

Figure 5: TA15 model magnetic field data. In each case, plotted is Y vs B_x [GSM], (at X=−14.9 R_E, i.e. the X position of C1 at ~00:28 UT on 12 Oct 2006), with the TA15 modelled B_y value shown by the color bar on the right. The black triangle shows the Y-location of C1, at B_x = 0. In panel (a) we have imposed IMF B_y = 0, and for panel (b) we have used the 1-hour mean-averaged IMF B_y (+1.56 nT) in the hour prior to 00:28 UT.

To aid in this interpretation, we present TA15 model magnetic field data in Figure 5, to provide an indication of the expected background B_y-component at the time of our interval. These data, from X = −14.9 R_E, are plotted against Y [GSM]-position on the horizontal axis, and against the B_x-component on the vertical axis. We have reversed the conventional direction of the horizontal axis (negative to positive from left to right) to be consistent with a view looking earthward from downtail. In panel (a) we show the field for the case that IMF B_y = 0 and in panel (b) the case that IMF B_y = +1.56 nT (the 1-hour mean-averaged IMF B_y in the hour prior to 00:28 UT). The first conclusion we can make from consideration of the B_y component in Fig. 5a is how, even under no IMF B_y penetration, a 'background' B_y value will exist in the tail purely dependent on location. In such a 'symmetric' tail, one would expect the background B_y value to appear as one moves away from midnight toward the dusk-dawn flanks, as well as further above and below the neutral sheet. Pre-midnight, we would expect to observe negative B_y above the neutral sheet (B_x > 0), and positive B_y below the

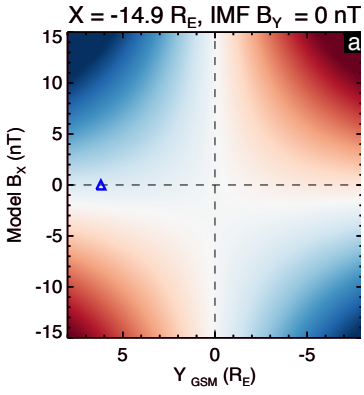

Deleted:

Deleted: blue

Deleted:

Deleted: ure

neutral sheet ($B_x < 0$), with the opposite effect post-midnight. This is the well known magnetotail flaring effect (Fairfield, 1979).

The data in Fig. 5a also show the effect of the negative (tailward) dipole tilt (as appropriate to our study interval) and current sheet warping on the local B_y component. According to Petrukovich (2011), the current sheet warping (controlled by the dipole tilt) is expected to add a negative B_y component pre-midnight and a positive B_y component post-midnight. Furthermore, the 'even tilt' effect is expected to add a negative B_y component to both the pre and post-midnight sectors for a negative tilt. This leads to the effect seen in Fig. 5a where in the pre-midnight sector, the location of the B_y polarity change occurs in the southern hemisphere (at $B_x \approx -3$ nT).

Fig. 5b illustrates the scenario relevant to our case study, where we have additionally a global positive IMF B_y penetration. This additional positive B_y has the effect of moving the location of the pre-midnight B_y polarity change back up towards the neutral sheet. This explains why the Cluster spacecraft observed $B_y \approx 0$ at times of $B_x \approx 0$ during the few tens of minutes prior to our interval, as noted in section 3.2. This also explains why C2-3 and C4 observed the polarity of B_y that they did throughout the interval. It is thus clear that positive IMF B_y penetration does not mean we should expect to observe positive B_y everywhere in the tail, rather, it simply means that there is expected to be some positive B_y perturbation to the already present 'background' B_y at a particular location. As Fig. 5b demonstrates, C2 and C4 (located above the neutral sheet) are expected to have observed negative B_y even though positive IMF B_y has penetrated into the magnetotail, illustrating that the flaring effect is generally dominant at the spacecraft location. The background B_y expected at their location (pre-midnight, $B_x > 0$), is negative and the IMF B_y -associated perturbation was not large enough to enforce a sign change in B_y.

The Cluster spacecraft in our study were all located pre-midnight (+Y GSM). From Figure 3, C2 and C4 observed positive B_x, and negative B_y, and at ~00:28 UT were located at around Z = −1 R_E (Figure 1). C3, however, observed negative B_x and positive B_y, and was located at around Z = −2.5 R_E. The location of the neutral sheet at ~00:28 UT can therefore be said (locally) to have been somewhere between −1 and −2.5 R_E in Z. C1 was located at around Z =

Deleted: effect

Deleted: ure

Deleted: ure

Deleted: ure

Deleted: when

Deleted: at times of

Deleted: ure

Deleted: .

Deleted: crossing

−1.5 R_E and, throughout the five-minute interval, observed a B_x which continually fluctuated from positive to negative, yet observed mostly weakly negative B_y. For B_y to have remained negative, despite C1 moving above and below the neutral sheet, suggests that there was a B_y negative 'kink' in the magnetotail that was localized to the vicinity of C1. This is further supported by the fact that numerous (albeit brief) positive B_y excursions occurred when C1 was above the neutral sheet (as noted in section 3.2). We use the term 'kink' to highlight a deformation in the nearby field lines which results in the observed perturbations to the local B_y component. We suggest that this deformation could be relatively small in terms of field line length, much like a kink in a cable or wire. In the following section, we investigate this kink in relation to the observed current sheet flapping.

4.3 Evidence for current sheet flapping as a source of the asymmetric flows

If a localized magnetic field perturbation was associated with the lack of observation of the expected dusk-dawn flow for magnetotail untwisting, investigating its cause seems a worthwhile endeavour. The clear sinusoidal-like variation in B_x observed by C1, which is evidence of current sheet flapping (e.g. Runov et al., 2009), provides us with a starting point for this investigation. This flapping must be highly localized as at the time of our five-minute flow interval (00:28 -00:33 UT), only C1 observed the flapping. MVA analysis (Sonnerup & Cahill, 1967) suggests that the flapping was a kink-like wave which was propagating dawnward (Rong et al., 2015; Wu et al., 2016), and therefore may have been a source of the observed dusk-dawn flow.

The causes of current sheet flapping have been discussed previously (Runov et al., 2009; Wei et al., 2019). One such cause has been attributed to localized, periodical reconnection – a process known to drive Bursty Bulk Flows (BBFs) in the magnetotail (Angelopoulos et al., 1994; Zhang et al., 2016). In fact, BBFs excited directly as a result of reconnection in the tail have been previously linked to magnetic fluctuations in the current sheet (Nakamura et al., 2009; Wu et al., 2016). Examining the data presented in Fig. 3 iii) and Fig. 3 iv), we note that C1 measured a generally positive B_z, with a few negative blips, as well as continually fast (v_x > 200 km s^{-1}) earthward flow, peaking at over 370 km s^{-1} with bursts of enhanced convective flow ($v_{\perp x}$ > 200 km s^{-1}) also apparent. These observations are fairly consistent

Deleted: ure

Deleted: Figure

with (if slightly slower than) the original definition of a BBF (Angelopoulos et al., 1994). This, along with the absence of similar flow observations in the C3 data, suggests that C1 may have been located earthward of a localized reconnection site (owing to $B_z > 0$), where persistent, localized reconnection was exciting fast earthward flow. The reconnection process may then have been driving the current sheet flapping, inducing the localized kink in the field, and ultimately controlling the dusk-dawn direction of the convective flow.

It is well known that the magnetic tension force is responsible for the acceleration of plasma following reconnection (Karlsson et al., 2015). Our observations of a dusk-dawn flow component may be related to the localized magnetic tension forces driving and directing plasma flows in association with the flapping. In order to provide some scope to this suggestion, we attempted to find the direction of the $\boldsymbol{J} \times \boldsymbol{B}$ forces acting on the plasma. We used the curlometer technique (Dunlop et al., 1988, 2002), to estimate the average current density, $\boldsymbol{J}$, flowing through the volume bound by the spacecraft tetrahedron. The $\boldsymbol{J} \times \boldsymbol{B}$ force density [N m^{-3}] is then calculated, firstly, by taking the cross product of $\boldsymbol{J}$ with the average magnetic field vector $\boldsymbol{B}$ from the four-spacecraft ($\boldsymbol{B}_{AVG}$). We also calculate $\boldsymbol{J} \times \boldsymbol{B}$ using solely $\boldsymbol{B}$ from C1 ($\boldsymbol{B}_{C1}$), in order to provide a more local estimate for $\boldsymbol{J} \times \boldsymbol{B}$ at the location of C1.

In order to check the validity of using the curlometer approach, we calculated the quality parameter, Q, defined as $|\nabla . \boldsymbol{B}|/|\nabla \times \boldsymbol{B}|$. It is generally accepted that a value of $Q < 0.5$ is required for a current estimate to be valid. Hence, the value of Q, along with due consideration of the spacecraft configuration and its orientation relative to the magnetic field structure, may be used as a monitor of how reliable the curlometer approach is (Dunlop et al., 2002). This is discussed further below, in reference to the analysis shown in Figure 6.

Deleted:

Deleted: (Karlsson et al., 2015)

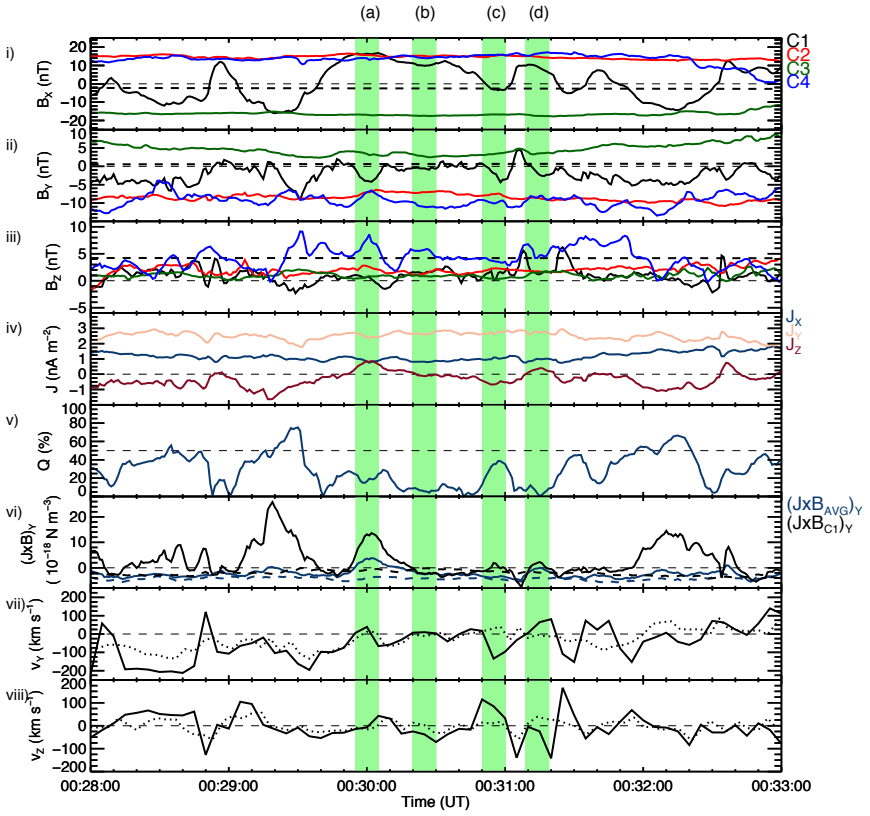

Figure 6: i-iii) The local magnetic field vector $\boldsymbol{B}$ (B_x, B_y, B_z) observed by C1-4, as shown previously (solid lines) and the TA15 modelled $\boldsymbol{B}$ vector for C1 (dashed black lines). iv) The components of the current density vector $\boldsymbol{J}$ (J_x, J_y, J_z), v) Q, vi) $(\boldsymbol{J} \times \boldsymbol{B}_{AVG})_Y$ (solid blue line) and $(\boldsymbol{J} \times \boldsymbol{B}_{C1})_Y$ (solid black line). The dashed blue and black lines indicate the equivalent calculation where the TA15 model $\boldsymbol{B}$ field of C1 has been used (see text). vii) v_y ($v_{\perp y}$ in solid lines), observed by C1 and viii) v_z ($v_{\perp z}$ in solid lines), also observed by C1. The green highlighted regions labelled (a), (b), (c) and (d) correspond to four specific time-windows of interest (discussed in-text).

Shown in Fig. 6 i-iii) are the local magnetic field B_x, B_y and B_z components, as presented previously. In Fig. 6 iv) are the current density J_x, J_y and J_z components determined from the

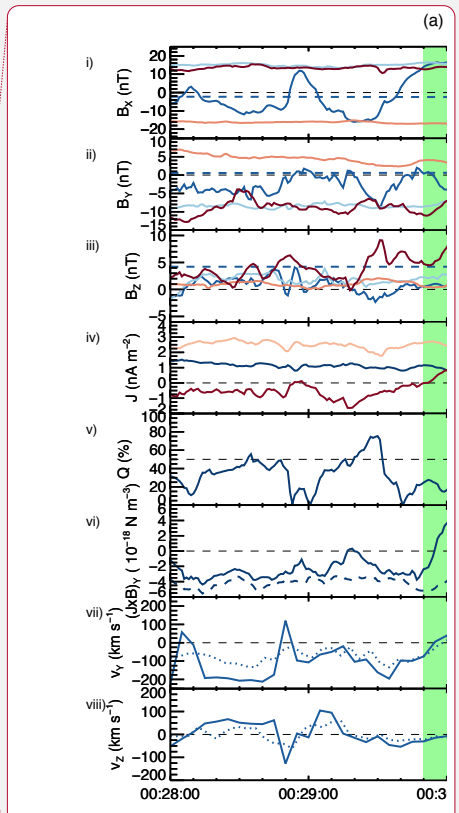

Deleted:

Deleted: ue

Deleted: ***B***

Deleted: ***B***

Deleted: computed using the TA15 modelled C1 ***B*** (dashed line, discussed in-text),

Deleted: ure

Deleted: ure

curlometer analysis. In Fig. 6 vi) is the dusk-dawn component of $\boldsymbol{J} \times \boldsymbol{B}_{AVG}$ and $\boldsymbol{J} \times \boldsymbol{B}_{C1}$. Finally, in Fig. 6 vii) and viii) are the dusk-dawn and north-south components of the flow (and field-perpendicular flow) observed by C1, as shown previously. In panels (i-iii), the dashed black line represents the TA15 modelled magnetic field (see section 4.2) at the location of C1. In panel (vi) the dashed blue and black lines represent the $(\boldsymbol{J} \times \boldsymbol{B}_{AVG})_Y$ and $(\boldsymbol{J} \times \boldsymbol{B}_{C1})_Y$ forces, respectively, where $\boldsymbol{J}$ and $\boldsymbol{J} \times \boldsymbol{B}$ have been computed using the model field at the location of C1 and the true magnetic fields measured by C2-C4. These 'model $(\boldsymbol{J} \times \boldsymbol{B})_Y$ forces' have been computed to provide an illustration of what one would expect the 'unperturbed' magnetic field of C1 and the associated $(\boldsymbol{J} \times \boldsymbol{B})_Y$ force to look like, in the absence of any dynamical effects such as current sheet flapping or field line 'kinking'. In both cases, the model $(\boldsymbol{J} \times \boldsymbol{B})_Y$ forces are weakly dawnward, consistent with the 'background curvature' of the magnetic field at this pre-midnight location (see Fig. 7). Fig. 6 v) suggests that our curlometer approach is generally appropriate, as Q mostly remains below 50% (horizontal dashed line) for the five-minute interval. We note that, unlike in previous studies which have used the curlometer technique at inter-spacecraft separation distances of << 1 R_E (e.g. Dunlop et al., 2002; Runov et al., 2003), in our case the Cluster spacecraft separation is large ($\gtrsim$ 1 R_E). Therefore, the curlometer is likely to be an underestimate of the true current at these scale sizes. Critically, however, the spacecraft configuration is such that the estimate of the direction of the currents should be stable. Thus, although the volume enclosed by the spacecraft is greater than the scale sizes of the current sheet flapping and kink, a reliable estimate of the direction of the net $\boldsymbol{J} \times \boldsymbol{B}$ force within the enclosed volume may still be obtained.

Two key features of Figure 6 are apparent. Firstly, it appears as though the perturbations to $(\boldsymbol{J} \times \boldsymbol{B})_Y$ are mostly associated with the magnetic field perturbations generally only observed by C1. This is made apparent by comparing $(\boldsymbol{J} \times \boldsymbol{B}_{C1})_Y$ with $(\boldsymbol{J} \times \boldsymbol{B}_{AVG})_Y$, where the perturbations are much larger in magnitude for $(\boldsymbol{J} \times \boldsymbol{B}_{C1})_Y$. We also note that both $(\boldsymbol{J} \times \boldsymbol{B}_{AVG})_Y$ and $(\boldsymbol{J} \times \boldsymbol{B}_{C1})_Y$ are effectively always positive with respect to their model equivalents. However, $(\boldsymbol{J} \times \boldsymbol{B}_{AVG})_Y$ is still mostly net negative whereas $(\boldsymbol{J} \times \boldsymbol{B}_{C1})_Y$ is net positive. This suggests that using $\boldsymbol{B}_{C1}$, rather than $\boldsymbol{B}_{AVG}$ in calculating $(\boldsymbol{J} \times \boldsymbol{B})_Y$ has overall

Deleted: ure
Deleted: $\boldsymbol{B}$
Deleted: .
Formatted: Font: Not Bold
Deleted: In panels i-iii) and vi), also shown is a dashed blue line. …
Deleted: this
Deleted: is
Deleted: s
Deleted: $\boldsymbol{J} \times \boldsymbol{B}$
Deleted:
Deleted: the average $\boldsymbol{B}$ have
Deleted: , hereafter referred to as the
Deleted: '.
Deleted: This has
Deleted: ure
Formatted: Font color: Auto
Deleted: , displayed in Figure 6 vi),

776 reduced the effects of the larger-scale background field curvature (incorporated by
777 including the other spacecraft). Second, the magnetic field and flow dynamics evident in Fig.
778 6 appear to almost always be associated with positive (duskward) enhancements in $(\boldsymbol{J} \times \boldsymbol{B})_y$,
779 in contrast to the model dawnward sense of $(\boldsymbol{J} \times \boldsymbol{B})_y$. This is particularly evident in the case
780 of $(\boldsymbol{J} \times \boldsymbol{B}_{C1})_y$, but also generally true in the case of $(\boldsymbol{J} \times \boldsymbol{B}_{AVG})_y$. We therefore suggest that
781 the dynamic behaviour of $(\boldsymbol{J} \times \boldsymbol{B})_y$ is simply consistent with the localised kinks and flapping
782 in the magnetic field that are associated with the transient perturbations to the dusk-dawn
783 flow observed by C1.
784
785
786 *4.4 Visualization of the observed dynamics*
787 In an effort to visualize these plasma sheet dynamics, we show in Figure 7 a series of
788 sketches that attempt to associate the observed magnetic field perturbations with the
789 observed dusk-dawn convective flows. The panels correspond to the four time-windows
790 indicated on Figure 6 by the highlighted regions labelled a-d. In each panel, we indicate the
791 approximate relative position of the 4 Cluster spacecraft in GSM coordinates, and the
792 appropriate sense of B_y measured by each spacecraft is shown by the purple arrows at each
793 spacecraft location (the Z-component of the field was in fact generally small, and has been
794 exaggerated here for illustrative purposes). We also superimpose nominal plasma sheet
795 field lines (again with an exaggerated extent in Z) that display the sense of B_y implied by the
796 TA15 data presented in Figure 5 (long blue curved arrows). The dashed lines represent the
797 location of the neutral sheet at the end of each time window. This is tilted slightly, as
798 appropriate for IMF $B_y > 0$, but with the end-state of the "flap" of the current sheet implied
799 by the sign of B_x observed by C1. In red is the perturbation to the field implied by the sign of
800 B_y observed by C1.
801

Deleted: Second, the dawnward flow bursts (reproduced in Fig. 6 vii) tend to occur when $(\boldsymbol{J} \times \boldsymbol{B})_y$ is more negative, with the weak duskward flow bursts occurring when $(\boldsymbol{J} \times \boldsymbol{B})_y$ is less negative. We note that there is not a one-to-one correlation between the $(\boldsymbol{J} \times \boldsymbol{B})_y$ and $v_{\perp y}$ data. This could well be due to the large volume over which $\boldsymbol{J} \times \boldsymbol{B}$ is being averaged and we make no attempt to interpret the detailed variations in $(\boldsymbol{J} \times \boldsymbol{B})_y$ implied by these data. However, as this region of space will contain the localized flapping and kink, the calculated $\boldsymbol{J} \times \boldsymbol{B}$ should be influenced by these dynamics and hence still provide an indication of the forces acting within that region. The consistency between the direction of $(\boldsymbol{J} \times \boldsymbol{B})_y$ and $v_{\perp y}$ therefore suggests that the $\boldsymbol{J} \times \boldsymbol{B}$ force associated with the current sheet flapping is exerting some level of control over the direction of the convective flow. We also note that the $(\boldsymbol{J} \times \boldsymbol{B})_y$ force is effectively always less negative than the model $(\boldsymbol{J} \times \boldsymbol{B})_y$ force. As can be seen in Figure 6 vi), the model $(\boldsymbol{J} \times \boldsymbol{B})_y$ force is acting steadily dawnward, consistent with the duskward location of the spacecraft and suggesting that the curlometer analysis is simply picking up the $(\boldsymbol{J} \times \boldsymbol{B})_y$ force associated with the 'background curvature' of the magnetic field. Thus, we suggest that the positive deviations of $(\boldsymbol{J} \times \boldsymbol{B})_y$ from the model $(\boldsymbol{J} \times \boldsymbol{B})_y$ force are due to the perturbations (flapping and kinking) observed by C1.¶

Formatted: Font color: Auto

Deleted: -

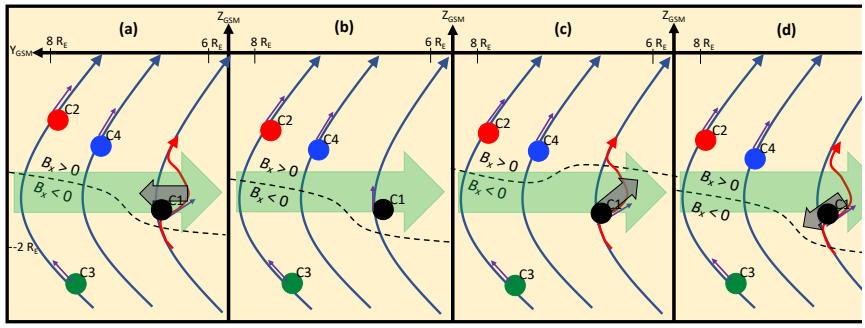

Deleted:

Figure 7: Schematic diagrams of the observed magnetic field perturbations and dusk-dawn convective flows during the time-windows indicated in Fig. 6 by the highlighted regions. The approximate locations of the four Cluster spacecraft relative to one-another in the Y-Z GSM plane are indicated (not to scale) by the colored circles. The curved blue arrows represent magnetic field lines, and the short purple arrow indicates the local sense of B_y at the location of each spacecraft. The dashed black line indicates the current sheet. In panels (a), (b) and (d), the curved red arrow shows the 'kinked' magnetic field line. The long thick green arrow shows the direction of the model $(\boldsymbol{J} \times \boldsymbol{B})_y$ force associated with the background curvature of the magnetic field, and the small thick gray arrow shows the direction of the dusk-dawn convective flow observed by C1.

In Fig. 7a C1 is located above the current sheet and measured negative B_y. A weakly duskward convective flow was observed at this time (as indicated by the thick gray arrow), consistent with the duskward sense of the $(\boldsymbol{J} \times \boldsymbol{B})_y$ force, and opposite to the sense of the model $(\boldsymbol{J} \times \boldsymbol{B})_y$ force associated with the background curvature of the magnetic field. In Fig. 7b, C1 is still above the current sheet but measured $B_y \approx 0$ and no dusk-dawn convective flow. In Fig. 7c C1 is shown below the current sheet, where the background B_y would be positive (see Fig. 5b). C1 instead observed an increasingly negative B_y, which we suggest is associated with the presence of the kink in the field. At the same time, C1 also observed a convective plasma flow with dawnward and slightly upward (+Z) component (thick gray

Deleted: Figure

Deleted: Figure

Deleted: Figure

arrow). We therefore suggest that the flow was associated with the upward/dawnward flap of the current sheet, and that the dawnward sense of the flow likely also resulted in the increase in negative B_y seen during the time-window shown in Fig. 6c. The positive $(\boldsymbol{J} \times \boldsymbol{B}_{C1})_y$ at this time, whilst inconsistent with the dawnward sense of the flow, is therefore consistent with the curvature of the magnetic field associated with the kink. $(\boldsymbol{J} \times \boldsymbol{B}_{AVG})_y$, meanwhile, was negative, likely due to incorporating the larger-scale background curvature of the magnetic field observed by the other spacecraft. In Fig. 7d C1 is shown above the current sheet, where it observed a weakly negative B_y. In this case, C1 observed a convective plasma flow with duskward and slightly downward (−Z) component. Similarly to in Fig. 7a, this flow occurred in concert with a positive enhancement in $(\boldsymbol{J} \times \boldsymbol{B})_y$ relative to the model $(\boldsymbol{J} \times \boldsymbol{B})_y$. This flow would therefore seem to be associated with the downward flap of the current sheet, and its duskward sense could indicate that it is acting to reduce the negative kink in B_y that is apparent over the time-window shown in Fig. 6d.

Whilst we acknowledge a degree of uncertainty in the details of the interpretation presented above of the specific relationship between the flows and the field, it serves to illustrate three observations about this interval of which we can be very certain: 1) The IMF, ionospheric convection, and comparison of the plasma sheet magnetic field observations to the TA15 model field, all lead to the expectation of an IMF $B_y > 0$ large-scale asymmetry in the magnetosphere. 2) The Cluster 1 spacecraft observed convective flow with a dusk-dawn component that was inconsistent with current theories of IMF B_y-induced dusk-dawn flows associated with magnetotail untwisting. We therefore note that the observations presented here cannot be attributed to the current model of large-scale magnetotail untwisting. 3) Magnetic field perturbations that were indicative of a localized current sheet flapping and dusk-dawn kink in the field occurred coincident with the flows. It therefore seems likely that in this case the IMF B_y-driven asymmetry was insufficient to override the localised dynamics in governing the dusk-dawn component of the flow.

Deleted: Figure

Deleted: i

Deleted: Figure

Deleted: Figure

Deleted: Figure

Deleted:

Formatted: Font: Italic

Formatted: Font: Italic, Subscript

Deleted: IMF B_y-driven asymmetries are not the only mechanism by which a dusk-dawn component may be introduced into the convective flow, with other dynamical processes also likely to contribute.

Deleted: ¶

¶

5. Summary

We have presented a case study from 12 October 2006 revealing a dynamic interval of plasma flows and current sheet flapping, observed by the Cluster 1 spacecraft. The key observations presented in this study may be summarised as follows:

- The OMNI data revealed that the IMF B_y had been positive for several hours prior to our interval of Cluster data, with the exception of three short-lived negative excursions.
- The SuperDARN ionospheric convection observations revealed a large-scale asymmetry consistent with IMF $B_y > 0$.
- C1 observed a changing B_x magnetic field component and associated duskward ($v_{\perp y} > 0$) flow when in the northern magnetic hemisphere, and dawnward ($v_{\perp y} < 0$) flow in the southern magnetic hemisphere.

Contrary to the results of a number of previous studies in the literature, during this particular interval, the dusk-dawn sense of the convective magnetotail flows ($v_{\perp y}$); and in particular, the dawnward flow observed in the southern hemisphere, does not agree with expectations based on the theoretical understanding of global magnetotail untwisting and the prevailing positive IMF B_y conditions, nor to expectations based on the location of the spacecraft and associated magnetotail flaring. We instead attribute the flows to a localized magnetic field perturbation, or 'kink' in the magnetotail, which appears to have been independent of any large-scale dynamics and may have instead been related to the observed current sheet flapping. We attributed the current sheet flapping to being driven by localized reconnection, itself inferred from the presence of the observed bursty fast earthward flow ($v_{\perp x} \approx 200$ km s^{-1}). Analysis using the curlometer technique suggests that the $(\boldsymbol{J} \times \boldsymbol{B})_y$ force is consistent with the localised kinks and flapping in the magnetic field that are associated with the transient perturbations to the dusk-dawn flow observed by C1.

Deleted: ,

Deleted: nor to expectations based on the location of the spacecraft and associated magnetotail flaring

Deleted: s

Deleted: have

Deleted: en

Deleted: dynamics

Deleted: instead

Deleted: that the $\boldsymbol{J} \times \boldsymbol{B}$ force associated with the current sheet flapping could have been exerting a level of control over the convective flow responsible for introducing the observed dusk-dawn component.

Although evidence for the large-scale penetration of IMF $B_y > 0$ is apparent, the IMF $B_y > 0$ penetration at the location of C1 appears to have been unable to override the variable dusk-dawn flow associated with the current sheet flapping. Further studies by the authors are currently underway to determine if such flows are a frequent occurrence, and to consider, and account for, localized tail dynamics more fully in a statistical analysis of the magnetotail flows.

Deleted: Whilst it is known that variable dusk-dawn flow can occur in conjunction with current sheet flapping, thisAlthough…

Deleted: is apparent

Deleted: .

Deleted: This seems to have case study has provided direct evidence that flapping can locally override the expected IMF B_y control of dusk-dawn magnetotail flow, in spite of clear global penetration of IMF $B_y > 0$; consequently, resultinged in the production of localized flows that do not agree with the expected direction for globalbased on the location and magnetotail untwisting considerations discussed above.

Deleted: such flows are

Acknowledgements

The authors would like to thank the FGM and CIS teams as part of the Cluster mission and acknowledge the Cluster Science Archive (Laakso et al., 2010) as the source of the Cluster data. We also wish to thank the OMNIWeb as the source of the solar wind and IMF data. The authors acknowledge the use of SuperDARN data. SuperDARN is a collection of radars funded by national scientific funding agencies of Australia, Canada, China, France, Italy, Japan, Norway, South Africa, United Kingdom, and United States of America, and we thank the international PI team for providing the data. The authors acknowledge access to the SuperDARN database via BAS data mirror (http://bslsuperdarnc.nerc-bas.ac.uk:8093/docs/) and are grateful for use of the Radar Software Toolkit (RST v4.2 https://zenodo.org/record/1403226#.Xy0u7y3MxTY) with which the raw radar data were processed. We acknowledge the WDC for Geomagnetism, Kyoto, for use of the auroral electrojet indices, which may be obtained from http://wdc.kugi.kyoto-u.ac.jp/aedir/. We are also grateful to Haje Korth for providing the IDL Geopack DLM containing the Tsyganenko magnetic field model routines and coordinate system conversions and wish to thank Nikolai Tsyganenko for useful discussion of his magnetic field models. Finally, we are thankful for the advice of Malcolm Dunlop regarding the applicability of the curlometer technique at large spacecraft separations. This research was undertaken with the support of funding from the following sources: Lancaster University Faculty of Science and Technology studentship (JHL), STFC Consolidated grant no. ST/R000816/1 (NAC, AG), NERC standard grant nos. NE/P001556/1 and NE/T000937/1 (MTW, AG).

References

Angelopoulos, V., Baumjohann, W., Kennel, C. F., Coroniti, F. V., Kivelson, M. G., Pellat, R., Walker, R. J., Lühr, H. and Paschmann, G. (1992). Bursty bulk flows in the inner central plasma sheet. *J. Geophys. Res., 97 (A4),* 4027-4039. doi:10.1029/91JA02701

Angelopoulos, V., Kennel, C. F., Coroniti, F. V., Pellat, R., Kivelson, M. G., Walker, R. J., Russell, C. T., Baumjohann, W., Feldman W. C. and Gosling, J. T. (1994). Statistical characteristics of bursty bulk flow events. *J. Geophys. Res., 99 (A11)*, 21,257-21,280. doi:10.1029/94JA01263

Balogh, A., Carr, C. M., Acuña, M. H., Dunlop, M. W., Beek, T. J., Brown, P., Fornacon, K. -H., Georgescu, E., Glassmeier, K. -H., Harris, J., Musmann, G., Oddy, T. and Scwingenschuh, K.

(2001). The Cluster magnetic field investigation: Overview of in-flight performance and initial results. *Ann. Geophys., 19,* 1207-1217. doi: 10.5194/angeo-19-1207-2001

Baumjohann, W., Paschmann, G. and Cattell, C. A. (1989). Average Properties in the Central Plasma Sheet. *Journal of Geophysical Research, 94 (A6),* 6597-6606. doi: 10.1029/JA094iA06p06597

Browett, S. D., Fear, R. C., Grocott, A., and Milan, S. E. (2017). Timescales for the penetration of IMF B_y into the Earth's magnetotail. *J. Geophys. Res.: Space Physics, 122 (1)*, 579-593. doi:10.1002/2016JA023198

Cao, J. B., Ma, Y. D., Parks, G., Rème, H., Dandouras, I., Nakamura, R., Zhang, T. L., Zong, Q., Lucek, E., Carr, C. M., Liu, Z. X. and Zhou, G. C. (2006). Joint observations by Cluster satellites of bursty bulk flows in the magnetotail. *J. Geophys. Res., 111 (A4),* A04206. doi:10.1029/2005JA011322

Case, N. A., Grocott, A., Haaland, S., Martin, C. J., and Nagai, T. (2018). Response of the Earth's Neutral Sheet to Reversals in the IMF B_y component. *J. Geophys. Res., 123 (10),* 8206-8218. doi:10.1029/2018JA025712

Case, N. A. and Wild, J. (2012). A statistical comparison of solar wind propagation delays derived from multispacecraft techniques. *J. Geophys Res.*, *117 (A2)*, A02101, doi:10.1029/2011JA016946.

Chisham G., Lester, M., Milan, S. E., Freeman, M. P., Bristow, W. A., Grocott A., McWilliams, K. A., Ruohoniemi, J. M., Yeoman, T. K., Dyson, P. L., Greenwald, R. A., Kikuchi, T., Pinnock, M., Rash, J. P. S., Sato, N., Sofko, G. J., Villain, J. -P. and Walker, A. D. M. et al. (2007). A decade of the Super Dual Auroral Radar Network (SuperDARN): scientific achievements, new techniques and future directions. *Surveys in Geophysics 28,* 33-109. doi:10.1007/s10712-007-9017-8

Cowley, S. W. H. (1981). Magnetospheric asymmetries associated with the y-component of the IMF. Planet Space Sci, *29 (1)*, 79-96. doi:10.1016/0032-0633(81)90141-0

Dungey, J. W. (1961). Interplanetary magnetic field and the auroral zones. *Phys. Rev. Lett., 6*, 47-48. doi:10.1103/PhysRevLett.6.47

Dunlop, M. W., Southwood, D. J., Glassmeier, K. -H., and Neubauer, F. M. (1988). Analysis of multipoint magnetometer data. *Advances in Space Research, 8 (9-10),* 273-277. doi:10.1016/0273-1177(88)90141-X

Dunlop, M. W., Balogh, A., Glassmeier, K. -H. and Robert, P. (2002). Four-point Cluster application of magnetic field analysis tools: The Curlometer. *J. Geophys. Res., 107 (A11).* doi:10.1029/2001JA005088

Escoubet, C. P., Fehringer, M. and Goldstein, M. (2001). The Cluster Mission. *Ann. Geophys., 19,* 1197 – 1200. doi:10.5194/angeo-19-1197-2001

Fairfield, D. H. (1979). On the Average Configuration Of The Geomagnetic Tail. *J. Geophys. Res., 84 (A5),* 1950-1958. doi:10.1029/JA084iA05p01950

Frühauff, D. and Glassmeier, K.-H. (2016). Statistical analysis of magnetotail fast flows and related magnetic disturbances. *Ann. Geophys., 34,* 399-409. doi:10.5194/angeo-34-399-2016

Grocott, A. (2017). Time Dependence of Dawn-Dusk Asymmetries in the Terrestrial Ionospheric Convection Pattern. In: Haaland, S. et al. (2017), *Dawn-Dusk Asymmetries in Planetary Plasma Environments,* John Wiley and Sons, Inc., 107-123

Grocott, A., Yeoman, T. K., Nakamura, R., Cowley, S. W. H, Frey, H. U., Rème, H. and Klecker, B. J. (2004a). Multi-instrument observations of the ionospheric counterpart of a bursty bulk flow in the near-Earth plasma sheet. *Ann. Geophys., 22*, 1061-1075, 1432-0576/ag/2004-22-1061.

Grocott, A., Yeoman, T. K., Cowley, S. W. H, and Rème, H. (2004b). Multi-instrument observations of bursty bulk flows and their ionospheric counterparts. *Proc. Seventh Internat. Conf. on Substorms,* UDK-52-854, FMI, Helsinki, Finland, 107-110.

Grocott, A., Badman, S. V., Cowley, S. W. H, and Cripps (2004c). The influence of the IMF B_Y on the nature of the nightside high-latitude ionospheric flow during intervals of positive IMF B_Z. *Ann. Geophys., 22*, 1755-1764, doi:10.5194/angeo-22-1755-2004.

Grocott, A., Yeoman, T. K., Milan, S. E. and Cowley, S. W. H. (2005), Interhemispheric observations of the ionospheric signature of tail reconnection during IMF-northward non-substorm intervals, *Ann. Geophys., 23*, 1763–1770. doi:10.5194/angeo-23-1763-2005.

Grocott, A., Yeoman, T. K., Milan, S. E., Amm. O., Frey, H. U., Juusola, L., Nakamura, R., Owen, C. J., Rème, H. and Takada, T. (2007). Multi-scale observations of magnetotail flux transport during IMF-northward non-substorm intervals. *Ann. Geophys., 25*, 1709-1720. doi:10.5194/angeo-25-1709-2007

Grocott, A., Milan, S. E. and Yeoman, T. K. (2008). Interplanetary magnetic field control of fast azimuthal flows in the nightside high-latitude ionosphere, *Geophys. Res. Lett.,* 35, L08102, doi:10.1029/2008GL033545.

Haaland, S., Runov, A. and Forsyth, C. (2017). Dawn-Dusk Asymmetries in Planetary Plasma Environments, *Geophysical Monograph 230, First Edition. American Geophysical Union.* Published 2017 by John Wiley & Sons, Inc.

Karlsson, T., Hamrin, M., Nilsson, H., Kullen, A., and Pitkänen, T. (2015). Magnetic forces associated with bursty bulk flows in the Earth's magnetotail. *Geophys. Res. Lett., 42 (9),* 3122-3128. doi:10.1002/2015GL063999

Kiehas, S. A., Runov, A., Angelopoulos, V., Hietala, H. and Korovinksiy, D. (2018). Magnetotail Fast Flow Occurrence Rate and Dawn-Dusk Asymmetry at X_{GSM} ~ -60 R_E. *J. Geophys. Res.: Space Physics, 123 (3),* 1767 – 1778. doi:10.1002/2017JA024776

King, J. H., and Papitashvili, N. E. (2005). Solar wind spatial scales in and comparisons of hourly Wind and ACE plasma and magnetic field data. *J. Geophys. Res., 110*, A02104. doi:10.1029/2004JA010649

Kissinger, J., McPherron, R. L., Hsu, T. -S. and Angelopoulos, V. (2012). Diversion of plasma due to high pressure in the inner magnetosphere during steady magnetospheric convection. *J. Geophys. Res., 117,* A05206. doi:10.1029/2012JA017579

Khurana, K. K., Walker, R. J., and Ogino, T. (1996). Magnetospheric convection in the presence of interplanetary magnetic field By: A conceptual model and simulations. *J. Geophys. Res.*, *101 (A3)*, 4907–4916. doi:10.1029/95JA03673

Kubyshkina, D. I., Sormakov, D. A., Sergeev, V. A., Semenov, V. S., Erkaev, N. V., Kubyshkin, I. V., Ganushkina, N. Yu. And Dubyagin, S. V. (2014). How to distinguish between kink and sausage modes in flapping oscillations? *J. Geophys. Res., 119,* 3,002-3,015. doi:10.1002/2013JA019477.

Laakso, H., C. Perry, S. McCaffrey, D. Herment, A.J. Allen, C.C. Harvey, C.P. Escoubet, C. Gruenberger, M.G.G.T. Taylor, and R. Turner (2010), Cluster Active Archive: Overview, 3-37, The Cluster Active Archive, Astrophysics and Space Science Proceedings, H. Laakso et al. (eds.), Springer.

Lockwood, M. (1993), Modelling high-latitude ionosphere for time-varying plasma convection, IEE Proceedings-H, Vol. 140. No. 2. doi:10.1049/ip-h-2.1993.0015

Malova, H. V., Zelenyi, L. M., Popov, V. Y., Petrukovich, A. A. and Runov, A. V. (2007). Asymmetric thin current sheets in the Earth's magnetotail. *Geophys. Res. Lett., 34 (16),* L16108. doi:10.1029/2007GL030011

McPherron, R. L., Hsu, T. -S., Kissinger, J., Chu, X., and Angelopoulos, V., (2011). Characteristics of plasma flows at the inner edge of the plasma sheet. *J. Geophys. Res., 116 (A5)*, A00133. doi:10.1029/2010JA015923

Nakamura, R., Baumjohann, W., Klecker, B., Bogdanova, Y., Balogh, A., Rème, H., Bosqued, J. M., Dandouras, I., Sauvaud, J. A., Glassmeier, K. -H., Kistler, L., Mouikis, C., Zhang, T. L., Eichelberger, H. and Runov, A. (2002). Motion of the dipolarization front during a flow burst event observed by Cluster. *Geophys. Res. Lett., 29 (20), 1942.* doi:/10.1029/2002GL015763

Nakamura, R., Retinò, A., Baumjohann, W., Volwerk, M., Erkaev, N., Klecker, B., Lucek, E. A., Dandouras, I., André, M. and Khotyainstev, Y. (2009). Evolution of dipolarization in the near-Earth current sheet induced by Earthward rapid flux transport. *Ann. Geophys*., *27*, 1743-1754. doi:10.5194/angeo-27-1743-2009

Formatted: Font: Not Italic

Deleted: ,

Deleted: ,

1138 Ness, N. F. (1965). The Earth's Magnetic Tail. *J. Geophys. Res., 70 (13),* 2989–3005.
1139 doi:10.1029/JZ070i013p02989
1140
1141 Newell, P. T., Sotirelis, T., Liou, K., Meng, C. -I. and Rich, F. J. (2007). A nearly universal solar
1142 wind-magnetosphere coupling function inferred from 10 magnetospheric state variables. *J.*
1143 *Geophys. Res., 112 (A1),* A01206. doi: 10.1029/2006JA012025
1144
1145 Nishitani, N., Ruohoniemi, J. M., Lester, M., Baker, J. B. H., Koustov, A. V., Shepherd, S. G.,
1146 Chisham, G., Hori, T., Thomas, E. G., Makarevich, R. A., Marchaudon, A., Ponomarenko, P.,
1147 Wild, J. A., Milan, S. E., Bristow, W. A., Devlin, J., Miller, E., Greenwald, R. A., Ogawa, T. and
1148 Kikiuchi, T. (2019). Review of the accomplishments of mid-latitude Super Dual Auroral Radar
1149 Network (SuperDARN) HF radars. *Progress in Earth and Planetary Science*, *6:27*.
1150 doi:10.1186/s40645-019-0270-5
1151
1152 Ohma, A., Østgaard, N., Reistad, J. P., Tenfjord, P., Laundal, K. M., Moretto Jørgensen, T.,
1153 Haaland, S. E., Krcelic, P. and Milan, S. (2019). Observations of Asymmetric Lobe Convection
1154 for Weak and Strong Tail Activity. *J. Geophys. Res.: Space Physics, 124 (12).*
1155 doi:10.1029/2019JA026773
1156
1157 Pettigrew, E. D., Shepherd, S. G. and Ruohoniemi, J. M. (2010). Climatological patterns of
1158 high-latitude convection in the Northern and Southern hemispheres: Dipole tilt
1159 dependencies and interhemispheric comparisons. *J. Geophys., Res., 115*, doi:
1160 10.1029/2009JA014956.
1161
1162 Petrukovich, A. A. (2011). Origins of plasma sheet B_Y. *J. Geophys. Res., 116 (A7)*, A07217.
1163 doi:10.1029/2010JA016386
1164
1165 Petrukovich, A. A., Baumjohann, W., Nakamura, R., Schödel, R., and Mukai, T. (2001). Are
1166 earthward bursty bulk flows convective or field-aligned? *J. Geophys. Res., 106 (A10),* 21,211-
1167 21,215. doi:10.1029/2001JA900019
1168
1169 Petrukovich, A. A., Baumjohann, W., Nakamura, R., Runov, A., and Balogh, A. (2005). Cluster
1170 vision of the magnetotail current sheet on a macroscale. *J. Geophys. Res., 110 (A6),* A06204.
1171 doi:10.1029/2004JA010825
1172
1173 Pitkänen, T., Hamrin, M., Norqvist, P., Karlsson, T., and Nilsson, H. (2013). IMF dependence
1174 of the azimuthal direction of earthward magnetotail fast flows. *Geophys. Res. Lett., 40 (21)*,
1175 5598-5604. doi:10.1002/2013GL058136
1176
1177 Pitkänen, T., Hamrin, M., Norqvist, P., Karlsson, T., Nilsson, H., Kullen, A., Imber, S. M. and
1178 Milan, S. E. (2015). Azimuthal velocity shear within an earthward fast flow: further evidence
1179 for magnetotail untwisting? *Ann. Geophys., 33,* 245-255. doi:10.5194/angeo-33-245-2015
1180
1181 Pitkänen, T., Hamrin, M., Karlsson, T., Nilsson, H., and Kullen, A. (2017). On IMF B_Y-Induced
1182 Dawn-Dusk Asymmetries in Earthward Convective Fast Flows. In: Haaland, S. et al. (2017),
1183 *Dawn-Dusk Asymmetries in Planetary Plasma Environments,* John Wiley and Sons, Inc., 107-
1184 123.

Pitkänen, T., Kullen, A., Laundal, K. M., Tenfjord, P., Shi, Q. Q. Park. J. -S., Hamrin, M., De Spiegeleer, A., Chong, G. S. and Tian, A. M. (2019). IMF B_y Influence on Magnetospheric Convection in Earth's Magnetotail Plasma Sheet. *Geophys. Res. Lett., 46 (21),* 11,698-11,708. doi:10.1029/2019GL084190

Reistad, J. P., Østgaard, N., Tenfjord, P., Laundal, K. M., Snekvik, K., Haaland, S., Milan, S. E., Oksavik, K., Frey, H. U. and Grocott, A. (2016). Dynamic effects of restoring footprint symmetry on closed magnetic field lines. *J. Geophys. Res.: Space Physics, 121 (5)*, 015JA022058. doi:10.1002/2015JA022058

Reistad, J. P., Østgaard, N., Laundal, K. M., Ohma, A., Snekvik, K., Tenfjord, P., Grocott, A., Oksavik, K., Milan, S. E. and Haaland, S. (2018). Observations of asymmetries in ionospheric return flow during different levels of geomagnetic activity, *J. Geophys. Res.*, 123. doi:10.1029/2017JA025051

Rème, H., Bosqued, J. M., Sauvaud, J. A., Cros, A., Dandouras, J., Aoustin, C., Bouyssou, J., Camus, Th., Cuvilo, J., Martz, C., Médale, J. L., Perrier, H., Romefort, D., Rouzaud, J., d'Uston, C., Möbius, E., Crocker, K., Granoff, M., Kistler, L. M., Popecki, M., Hovestadt, D., Klecker, B., Paschmann, G., Scholer, M., Carlson, C. W., Curtis, D. W., Lin, R. P., McFadden, J. P., Formisano, V., Amata, E., Bavassano-Cattaneo, M. B., Baldetti, P., Belluci, G., Bruno, R., Chionchio, G., Di Lellis, A., Shelley, E. G., Ghielmetti, A. G., Lennartsson, W., Korth, A., Rosenbauer, H., Lundin, R., Olsen, S., Parks, G. K., McCarthy, M. and Balsiger, H. (1997). The Cluster Ion Spectrometry (CIS) Experiment. *Space Sci. Rev., 79*, 303-350. doi:10.1007/978-94-011-5666-0_12

Rong, Z. J., Barabash, S., Stenberg, G., Futaana, Y., Zhang, T. L., Wan, W. X., Wei, Y. and Wang, X. -D. (2015). Technique for diagnosing the flapping motion of magnetotail current sheets based on single-point magnetic field analysis. *J. Geophys. Res.: Space Physics, 120 (5),* 3462-3474. doi:10.1002/2014JA020973

Runov, A. Nakamura, R., Baumjohann, W., Zhang, T. L., Volwerk, M., Eichelberger, H. -U. and Balogh, A. (2003). Cluster observations of a bifurcated current sheet. *Geophys. Res. Lett., 30 (2),* 1036. doi:10.1029/2002GL016136

Runov, A., Angelopoulos, V., Sergeev, V. A., Glassmeier, K. -H., Auster, U., McFadden, J., Larson, D. and Mann, I. (2009). Global properties of magnetotail current sheet flapping: THEMIS perspectives. *Ann. Geophys., 27,* 319-328. doi:10.5194/angeo-27-319-2009

Ruohoniemi, J. M. and Baker, K. B. (1998). Large-scale imaging of high-latitude convection with Super Dual Auroral Radar Network HF radar observations. *J. Geophys. Res., 103 (A9),* 20,797-20,811. doi:10.1029/98JA01288

1230 Ruohoniemi, J. M. and Greenwald, R. A. (1996). Statistical patterns of high-latitude
1231 convection obtained from Goose Bay HF radar observations. *J. Geophys. Res., 101 (A10)*,
1232 21,743-21,763. doi:10.1029/96JA01584
1233
1234 Sergeev, V. A., Angelopoulos, V., Gosling, J. T., Cattell, C. A., and Russell, C. T. (1996).
1235 Detection of localized, plasma-depleted flux tubes or bubbles in the midtail plasma sheet. *J.*
1236 *Geophys. Res., 101 (A5),* 10,817 – 10,826. doi:10.1029/96JA00460
1237
1238 Sonnerup, B. U. Ö, and Cahill Jr, L. J. (1967). Magnetopause structure and attitude from
1239 Explorer 12 observations. *J. Geophys. Res., 72 (1),* 171-183.
1240 doi:10.1029/JZ072i001p00171
1241
1242 Sonnerup, B. U. Ö and Scheible, M. (1998). Minimum and Maximum Variance Analysis. In:
1243 Paschmann, G. and Daly, W. (1998), *Analysis Methods for Multi-Spacecraft Data,* pp 185-
1244 220, ESA Publications Division, Noordwijk, Netherlands.
1245
1246 Tenfjord, P., Østgaard, N., Snekvik, K., Laundal, K. M., Reistad, J. P., Haaland, S., and Milan, S.
1247 E. (2015). How the IMF B_y induces a B_y component in the closed magnetosphere and how it
1248 leads to asymmetric currents and convection patterns in the two hemispheres. *J. Geophys.*
1249 *Res.: Space Physics, 120 (11)*, 9368-9384. doi:10.1002/2015JA021579
1250
1251 Tenfjord, P., Østgaard, N., Strangeway, R., Haaland, S., Snekvik, K., Laundal, K. M., Reistad, J.
1252 P. and Milan, S. E. (2017). Magnetospheric response and reconfiguration times following
1253 IMF By reversals. *J. Geophys. Res.: Space Physics, 122 (1)*, 417-431.
1254 doi:10.1002/2016JA023018
1255
1256 Thomas, E. G. and Shepherd, S. G. (2018). Statistical Patterns of Ionospheric Convection
1257 Derived From Mid-Latitude, High-Latitude and Polar SuperDARN HF Observations. *J.*
1258 *Geophys. Res.: Space Physics, 123 (4),* 3196-3216. doi:10.1002/2018JA025280
1259
1260 Tsyganenko, N. A. and Andreeva, V. A. (2015). A forecasting model of the magnetosphere
1261 driven by an optimal solar wind coupling function. *J. Geophys. Res., 120 (10),* 8401-8425.
1262 doi:10.1002/2015JA021641
1263
1264 Volwerk, M., Zhang, T. L., Glassmeier, K. -H., Runov, A., Baumjohann, W., Balogh, A., Rème,
1265 H., Klecker, B. and Carr, C. (2008). Study of waves in the magnetotail region with cluster and
1266 DSP. *Advances in Space Research, 41 (10),* 1593-1597. doi:10.1016/j.asr.2007.04.005.
1267
1268 Wei, X. H., Cai, C. L., Cao, J. B., Rème, H., Dandouras, I., and Parks, G. K. (2015). Flapping
1269 motions of the magnetotail current sheet excited by nonadiabatic ions. *Geophys. Res. Lett.,*
1270 *42,* 4731-4735. doi:10.1002/2015GL064459
1271
1272 Wei, Y. Y., Huang, S. Y., Rong, Z. J., Yuan, Z. G., Jiang, K., Deng, X. H., Zhou, M., Fu, H. S., Yu,
1273 X. D., Xu, S. B., He, L. H. and Deng, D. (2019). Observations of Short-period Current Sheet
1274 Flapping Events in the Earth's Magnetotail. *The Astrophysical Journal Letters, 874,* 7pp.
1275 doi:10.3847/2041-8213/ab0f28/pdf.
1276

Wu, M., Lu, Q., Volwerk, M., Vörös, Z., Ma, X., and Wang, S. (2016). Current sheet flapping motions in the tailward flow of magnetic reconnection. *J. Geophys. Res., 121 (8),* 7817-7827. doi:10.1002/2016JA022819

Zhang, L. Q., Baumjohann, W., Wang, C., Dai, L., and Tang, B. B. (2016). Bursty bulk flows at different magnetospheric activity levels: Dependence of IMF conditions. *J. Geophys. Res., 121 (9)*, 8773-8789. doi:10.1002/2016JA022397